A model of roof-top surface pressures produced by conical vortices : Model development

D. Banks† and R. N. Meroney‡

Fluid Mechanics and Wind Engineering Program, Civil Engineering Department, Colorado State University(CSU), Fort Collins, CO 80523, U.S.A.

Abstract. The objective of this study is to understand the flow above the front edge of low-rise building roofs. The greatest suction on the building is known to occur at this location as a result of the formation of conical vortices in the separated flow zone. It is expected that the relationship between this suction and upstream flow conditions can be better understood through the analysis of the vortex flow mechanism. Experimental measurements were used, along with predictions from numerical simulations of delta wing vortex flows, to develop a model of the pressure field within and beneath the conical vortex. The model accounts for the change in vortex suction with wind angle, and includes a parameter indicating the strength of the vortex. The model can be applied to both mean and time dependent surface pressures, and is validated in a companion paper.

Key words: wind; vortex; load; pressure; roof; low-rise; building; flow separation.

1. Introduction

1.1. Correlation with upstream flow

It has long been established that the worst mean and peak suctions on flat low-rise building roofs occur for cornering or oblique wind angles (Kind 1986). These extreme suctions (Cp values below -10 are not uncommon) are the result of conical vortices which form along the roof edges (Fig. 1). The is essentially the same phenomenon that provides some 50% of the lift force to delta-wing aircraft; hence, the conical vortices are also known as "delta-wing" vortices.

Interest in the behaviour of these roof-top vortices has been heightened in part by the failure of quasi-steady (Q-S) theory to accurately predict the pressure fluctuations beneath the vortices (Letchford *et al.* 1993, Tieleman and Hajj 1995). This failure is of concern because the quasi-steady approach is the basis for many design codes. The Q-S theory combines information about upstream flow conditions with measured mean pressure coefficients to predict peak pressures via the equation (Cook 1990) :

$$Cp(t) = \left(\frac{U_{ref}(t)}{\overline{U_{ref}}}\right)^2 \cdot \overline{Cp}(\omega(t)) \tag{1}$$

† Now at CPP Inc.
‡ Professor

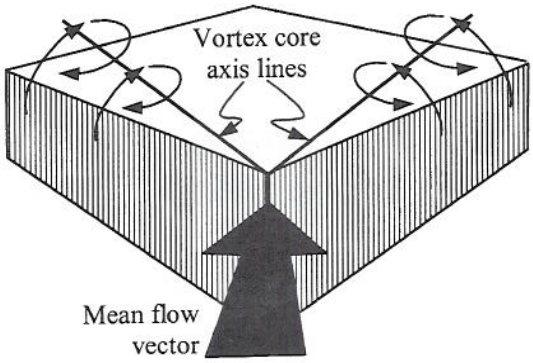

Fig. 1 Dual conical vortices in cornering wind

where ω = the wind direction and U_{ref} is the reference velocity. Links between the characteristics of upstream flow and the surface pressure have also been cited as an explanation for discrepancies between the rms and peak surface pressures measured under these vortices for full-scale tests and those measured for model scale tests. In particular, the need to correctly simulate lateral velocity fluctuations and small-scale turbulence intensity has been emphasized (Tieleman *et al.* 1998, Tieleman *et al.* 1994).

Several studies have examined the variation of surface pressure with upstream flow conditions. Roof suctions and upstream velocities were simultaneously measured for a flat roof low-rise model building (Kawai and Nishimura 1996). These authors concluded, based on the correlation of suction fluctuation over the entire roof, that the dual conical vortices sway in unison, and in concert with low frequency lateral turbulence. (Note that low frequency lateral velocity fluctuations could be seen as short-lived changes in wind direction.)

A connection has also been established between incident large scale/low frequency lateral turbulence and suction beneath the separated flow using frequency domain analyses (Hajj *et al.* 1997) and wavelet analysis on full-scale data from the Texas Tech University (TTU) (Jordan *et al.* 1997). However, these studies have not supplied substantiation of a connection between upstream small-scale lateral turbulence and surface pressure fluctuations.

One issue in performing such analyses is the position upstream at which the velocity measurements are recorded. Simultaneous upstream laser doppler anemometer (LDA) measurements of *u-v-w* velocity fluctuations have been compared with model surface pressures (Letchford and Marwood 1997). These flow velocity measurements were taken quite close to the building, at distances upstream from 2H to 0.1H, where H is building height. Conditional sampling was used to isolate the effects of instantaneous wind direction on *Cp* values. Their conclusion was that extremes in pressures were associated with large excursions in lateral velocity, specifically excursions toward a flow normal to the wall. Most significantly, this was only true for velocities measured less than 0.5H upstream. Even 2H is too far upstream for a good correlation between wind direction and surface pressure. It would appear that the building induced distortion of the oncoming flow fluctuations rapidly reduces any correlation between upstream flow and surface pressure. This is essentially why quasi-steady theory can not be validated for flow in the separation zones when $U(t)$ is measured upstream (Letchford and Marwood 1997). However, if the reference velocity $U_{ref}(t)$ is measured above the roof corner, quasi-steady theory gives good results for taps under the vortex (Zhao *et al.* 2000).

Given that only low-frequency upstream gusts have been directly connected to simultaneous

surface pressure fluctuations, and that the correlation between velocity (especially lateral velocity) fluctuations and surface pressure increases with proximity of flow measurement to the roof edge, it seems appropriate to focus on the mechanism by which the vortex transfers local velocity variations into surface pressure fluctuations. Once this is established, it is hoped that local flow conditions near the vortex can then be tied to the upstream flow parameters over a range of turbulence frequencies to provide a better understanding of how these parameters control surface pressure on low-rise buildings.

1.2. Connecting vortex flow structure to surface pressures

Velocities within the conical vortex have been measured using hot-wire probes, and the mean velocity fields documented (Kawai 1997). This work showed that the mean vortex core position, as defined by the centre of velocity field rotation, is located above the point of greatest mean rooftop suction. Banks, using simultaneous flow visualization and pressure measurement, has confirmed this, (though asymmetry in the pressure profile beneath the vortex shifts the point of highest mean suction slightly) (Banks *et al.* 2000). This work also demonstrated that at any instant in time, the peak suction remains directly beneath the moving vortex core.

Marwood and Wood (1997) made LDA measurements of velocities within the vortex and simultaneously sampled the surface pressure beneath the mean core position in smooth and turbulent flow. At each measurement location the velocities associated with the most negative 2.5% of the recorded *Cp*'s were extracted and averaged, creating a mean low *Cp* velocity field in a process called conditional sampling.

The results indicated that for $\overline{\omega} = 45°$, larger than average vortices produced the greatest surface suction. (In this paper, the wind angle relative to the roof edge along which the vortex in question has formed is $\omega = 90°$ for flow normal to that roof edge). These conditional sampling results are somewhat prejudiced by the use of a single pressure tap placed farther from the edge than the mean core position for $\overline{\omega} = 45°$. As a result, the lowest suction would tend to occur when the vortex core is directly above the tap, which requires a larger than average vortex. Nonetheless, the comparison of mean vortex position with mean and peak roof-pressure contours shows that larger than average vortices do provide greater suction for $\overline{\omega} = 45°$.

However, this only holds true for mean wind angles below 55° (Banks *et al.* 2000). For wind angles above 60°, the situation is reversed, and smaller-than-average vortices produce the peak suction. This is because the wind angle range known to produce the lowest mean *Cp*'s is $55° < \omega < 60°$ (Lin *et al.* 1995), and as both the studies of Banks and Marwood demonstrate, vortex size increases with wind angle. This indicates that the vortices producing the peaks tend to be similar in size to those found for $\omega = 55°$ to 60°, and that peak suctions for all wind angles could simply be due to momentary wind direction shifts toward that range. This is essentially what the quasi-steady theory assumes.

There is some reason to believe that vortex size is related to surface suction as more than an indicator of the current local wind direction. Low turbulence flow data from simultaneous flow visualization and surface pressure measurements taken at CSU indicates that even with the turbulence intensity below 4%, the vortices change size, possibly due to the influence of very small scale turbulence (Melbourne 1993), which could be produced at the leading edge itself. These low turbulence flow images demonstrated that smaller vortices actually produce higher surface suctions (Banks *et al.* 2000).

Marwood and Wood (1997) noted that "the mechanism linking vortex structure and surface pressure is little understood". We believe that inferences made regarding this mechanism, such as

those regarding the effect of vortex size above, can be improved if they are made in the context of a simple flow model. This study attempts to develop a model of the instantaneous link between flow in and around the recirculation area and the surface pressure beneath the vortex.

2. Existing surface pressure profile models

2.1. Point vortices in potential flow

Several authors (Kawai and Nishimura 1996, Marwood 1996), have compared the predictions of 2-D potential flow theory to the actual surface pressure profile along a line normal to the conical vortex axis. The results generally appear favourable in that the theoretical curve shape follows the data reasonably well.

These theoretical roof surface pressure profiles are based upon the flow field induced in potential flow theory by the placement of two counter-rotating vortices a distance $2h$ apart. The flat streamline between them is considered to be the roof surface (Fig. 2). The resulting surface flow velocity is given by

$$U(\xi)|_{z=0} = \frac{\Gamma h}{\xi^2 + h^2} \tag{2}$$

where Γ = circulation or strength of each vortex and $\xi = 0$ directly between the vortices. (Wilcox (1997) provides a good derivation of this formula.)

In order to apply potential flow theory, the flow must be incompressible ($\vec{\nabla} \cdot \hat{u} = 0$) and irrotational ($\vec{\nabla} \times \hat{u} = 0$, which implies $\hat{u} = \vec{\nabla} \cdot \phi$; it also implies inviscid flow). If the flow is also steady, the steady form of Bernoulli's equation can be used to predict the surface pressure along the ξ axis :

$$P = P_\infty - \frac{1}{2}\rho U^2(\xi) \tag{3}$$

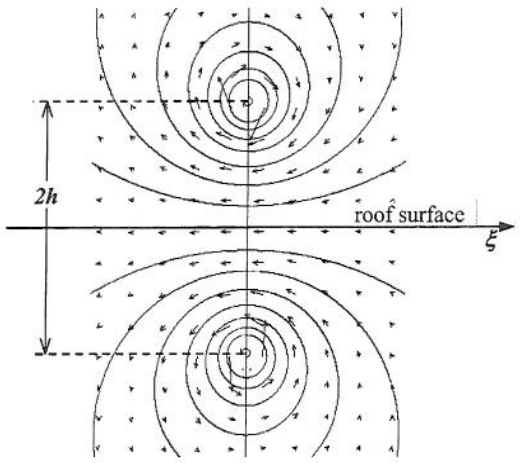

Fig. 2 Counter rotating vortices in 2-D potential flow, showing streamlines and velocity vectors. The flat streamline is taken to be the roof surface in this model.

where P_∞ is the static pressure when the flow stops, in the limit as $\xi \to \infty$ and $U \to 0$.

Let $\Delta P \equiv P - P_\infty = -\frac{1}{2}\rho\left(\frac{\Gamma \cdot h}{\xi^2 + h^2}\right)^2$, so that at $\xi = 0$ $\Delta P = \Delta P_{\min} = -\frac{1}{2}\rho(\Gamma/h)^2$.

The pressure distribution is now normalized by $\Delta P_{\min}$ to get

$$\frac{\Delta P}{\Delta P_{\min}} = \left(\frac{h^2}{\xi^2 + h^2}\right)^2 = \left(\frac{1}{(\xi/h)^2 + 1}\right)^2 \tag{4}$$

The vortex core height above the surface (h), has been measured from the flow visualization images, and used in Eq. (4). This procedure provides a reasonably good curve fit to aerospace data for swept delta wings with included angles less than 40° and tested at angles of attack above 20° (Greenwell and Wood 1992). For a building's square corner, with an included angle of 90° and an effective angle of attack we estimate at around 10° (depending on building height), the agreement is not as good. When actual values of h for roof-top vortex cores are used, it badly under-predicts the half width of the surface pressure profile (Banks *et al.* 2000).

To overcome this problem, a virtual core height is inferred from the pressure profile's half width: The half-height point on the $\Delta P / \Delta P_{\min}$ curve is selected, so that $\xi = \xi_{1/2}$ when $\Delta P / \Delta P_{\min} = 0.5$. By substituting $\Delta P / \Delta P_{\min} = 0.5$ and $\xi = \xi_{1/2}$ into Eq. (4), we get $h = 1.55\xi_{1/2}$. This virtual core height is often twice the actual core height.

In many implementations of Eq. (4), Cp is substituted for ΔP, so that $\xi = \xi_{1/2}$ at $Cp / Cp_{\min} = 0.5$, where $Cp_{\min}$ is the minimum Cp (i.e., the maximum suction) for a given x = constant line. This is not strictly correct, since

$$\frac{\Delta P}{\Delta P_{\min}} = \left(\frac{P - P_{ref} - \frac{1}{2}\rho U_{ref}^2}{P_{\min} - P_{ref} - \frac{1}{2}\rho U_{ref}^2}\right) = \left(\frac{Cp - 1}{Cp_{\min} - 1}\right), \text{ where } Cp \text{ is defined as}$$

$$Cp \equiv \frac{P - P_{ref}}{q} \tag{5}$$

The reason why Cp can be used in the place of ΔP in Eq. (4) is discussed in the next section.

The value of $Cp_{\min}$, rather than being calculated from vortex circulation, is, like the virtual height, extracted from the data. Hence, both input parameters (h and $Cp_{\min}$) are estimated from the data, and the model becomes essentially a curve fit to surface pressure data.

2.2. Rankine vortex based pressure profile

Cook's designer's guide provides a similar curve fit, based on the pressure profile through the core of a Rankine vortex (Cook 1990). A Rankine vortex features a fully viscous vortex core rotating as a solid body, surrounded by an irrotational, inviscid vortex (Fig. 3). The pressure coefficients for this flow are given by

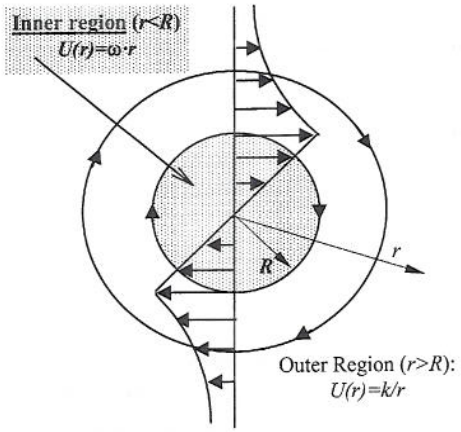

Fig. 3 Rankine vortex showing velocity profile through core

$$Cp_{inner} = Cp_o + \frac{U^2(r)}{U_{ref}^2} \text{ (from the integration of } \frac{dP}{dr} = \frac{\rho U^2}{r})$$

$$Cp_{outer} = 1 - \frac{U^2(r)}{U_{ref}^2} \text{ (from Bernoulli's equation)}$$

Matching the pressure coefficients at R gives

$$Cp_{inner}(R) = Cp_{outer}(R) = Cp_o + \frac{U_R^2}{U_{ref}^2} = 1 - \frac{U_R^2}{U_{ref}^2} \text{ so that } Cp_o = 1 - 2\frac{U_R^2}{U_{ref}^2}.$$

Since $U_{outer}(r) = k/r$, $U_R = k/R$ and $U_{inner}(r) = kr/R^2$, where k is a constant, the $Cp(r)$ formulae are

$$Cp_{outer} = 1 - \left(\frac{k}{r \cdot U_{ref}}\right)^2, \quad Cp_o = 1 - 2\left(\frac{k}{R \cdot U_{ref}}\right)^2, \text{ and}$$

$$Cp_{inner} = 1 - 2\left(\frac{k}{R \cdot U_{ref}}\right)^2 + \left(\frac{k \cdot r}{R^2 \cdot U_{ref}}\right)^2$$

This profile is then assumed to exist at the roof surface, so that $Cp_{\min}$ becomes Cp_o and r becomes ξ. As $\xi \to \infty$, $U(\xi) \to 0$, so that $Cp_{outer} \to 1$ and $Cp / Cp_{\min}$ approaches $1 / Cp_{\min}$. The same is true for the potential flow/point vortex model, since $\Delta P / \Delta P_{\min} \to 0$ as $\xi \to \infty$, which from Eq. (5) implies that $Cp \to 1$. However, the data measured in this study and elsewhere suggest that $Cp = 0$ or $Cp = -0.2$ is a more appropriate asymptote. The measured Cp values do not approach +1 when the flow appears to "stagnate" within the separation zone, as at the point of re-attachment. This is perhaps in part because the flow is really 3-dimensional, so that there is not a true stagnation, since $U_{axial} \approx U_{ref}$ at the point of reattachment (Marwood 1996). It could also be the result of the overall flow acceleration and curvature above the building, which reduces pressures over the whole roof as well as on the back wall.

Whatever the reason, the use of $Cp\,(\xi \to \infty) = 0$ as the asymptote simplifies the Rankine-based

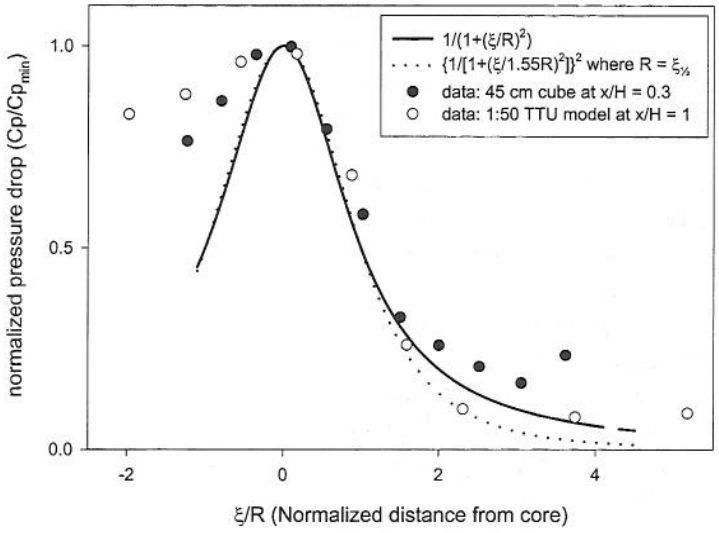

Fig. 4 Normalized *Cp* distributions under the vortex, normal to the roof edge

equations. If the value of *Cp* along the roof surface is considered to be reduced for all ξ by 1.0, then $Cp_{outer} = 0$ when $\xi \to \infty = 0$, since

$$Cp_{outer} = \left(\frac{k}{\xi \cdot U_{ref}}\right)^2, \quad Cp_{\min} = -2\left(\frac{k}{R \cdot U_{ref}}\right)^2 \text{ and } Cp_{inner} = -2\left(\frac{k}{R \cdot U_{ref}}\right)^2 \cdot \left(1 - \frac{1}{2}\frac{\xi^2}{R^2}\right) \text{ so that}$$

$$\left(\frac{Cp_{inner}}{Cp_{\min}}\right) = 1 - \frac{1}{2}\left(\frac{\xi}{R}\right)^2 \text{ and } \left(\frac{Cp_{outer}}{Cp_{\min}}\right) = \frac{1}{2}\left(\frac{R}{\xi}\right)^2$$

The model given in Appendix M of Cook's designer's guide approximates this relationship with the equation

$$\frac{Cp}{Cp_{\min}} = \frac{1}{(1 + A^2)} \text{ where } A = \xi / R \text{ and } \xi_{1/2} \text{ can be used for } R \tag{6}$$

In Fig. 4, the curves from Eqs. (4) and (6) are compared to mean data taken at CSU on a 1:50 model of the TTU Wind Engineering Research Field Laboratory (WERFL) building (Levitan and Mehta 1992) and on a larger 45 cm × 45 cm cubic model. The agreement is good in the region between the pressure peak and the roof centre, while the measured pressures remain significantly greater between the pressure peak and the leading edge.

2.3. Weaknesses of the surface pressure profile models

These models offer little insight into the manner in which the vortex controls suction on the roof surface. While the Rankine based model infers a surface profile similar to that through the vortex core, it does not attempt to describe the flow field. The potential flow model does describe the flow field, but it is actually misleading. The tangential velocity is predicted to increase infinitely (with $1/r$) as the vortex core is approached, and surface pressures are assumed to simply follow the Bernoulli

equation. For a mean Cp of −2.5, this requires a mean total velocity at the roof surface beneath the vortex of 1.9 times the mean upstream flow velocity at roof height (U_{ref}). Measurements taken for this study and elsewhere (Marwood 1996) indicate that the total velocity just above the surface in this case is usually quite close to U_{ref} (though much more turbulent, with more energy at higher frequencies).

For example, tap number 50501 on the TTU WERFL site roof is located at a normalized distance from the corner of $x/H = 0.36$, and at an angle with respect to the wall edge of $\phi = 14°$. Pressures measured at this tap are known to be quite low when it is beneath a conical vortex, with a mean Cp of −2.5 for $\omega = 60°$. Peak Cp's for tap 50501 for a test lasting 15 minutes are often around −11 (Cochran and Cermak 1992). This would require wind speeds of $U_S(t) = 3.5$ times $\overline{U}_{ref}$. Note that this implies winds speeds of over Mach 0.5 during a hurricane. This also implies a local gust of 1.85 times the mean local velocity, or 4.25 σ_U above the mean for a turbulence intensity of $\sigma_U/U = 20\%$.

The model which is developed in the following section demonstrates how Cp's of −11 can be achieved with wind speeds of only 2.4 times $\overline{U}_{ref}$, and gusts of only 1.6 times the mean local velocity (or $3\sigma_U$ above the mean for $\sigma_U/U = 20\%$). Unlike the models of Sections 2.1 and 2.2, this model produces a prediction of peak pressure beneath the vortex core based on the local flow conditions. This predicted peak suction could then be used as input into either of the symmetrical curve fits of the aforementioned models. However, given that the flowfield assumptions made by these models are inaccurate and that the shape of the surface pressure profile is generally asymmetric, the estimation of surface pressures near the peak can perhaps be better accomplished with a polynomial curve fit.

3. The vortex model

This section presents a model that emphasizes the interaction of the flow velocity above the vortex and the streamline curvature within the vortex in producing the low surface pressures. The model will be used to examine changes in Cp as a function of wind angle, distance from the apex, and local flow speed.

The nomenclature and overall flow pattern for the model are shown in Fig. 5. Instead of envisioning a flow field driven by a vortex, as in the potential flow model, we imagine the vortex to be like a wheel, being spun by the free stream at the point M. At the centre of the flow field model is a vortex similar to the Rankine vortex. The velocity profile associated with a Rankine vortex, shown in Figs. 3 and 6, is unrealistic, since the velocity will not change so abruptly as the circulating flow gradually changes from constant vorticity to zero vorticity. Instead, there will be a transition zone above the vortex in the shear layer, also shown in Fig. 6. In between the transition region and the core, experimental measurements (Marwood 1996) and numerical solutions (full Navier Stokes above a delta wing (Rizzi and Muller 1989)) show that the velocities within the real vortex core can be approximated by a power law profile. The viscous inner region is probably reduced to a very small area near the core ($r/h < \sim 0.2$). Above the transition region, the rotating flow merges with the free stream, so that U approaches U_{ref} instead of 0.

The pressure changes which occur towards the core (the point O) and the surface (the point S) are associated with centrifugal accelerations, $-mU^2/r$; hence, the local governing equation is

$$\frac{dP}{dn} = \frac{\rho U^2}{R_c} \tag{7}$$

where n is the unit normal to the curvature, R_c is the radius of curvature, and U is the fluid speed in the direction of vortex rotation.

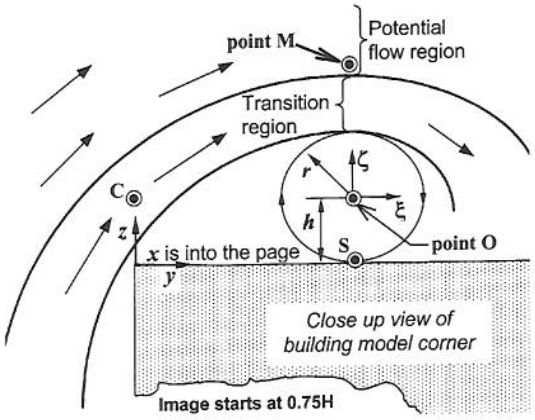

Fig. 5 Two-dimensional depiction of vortex flow model

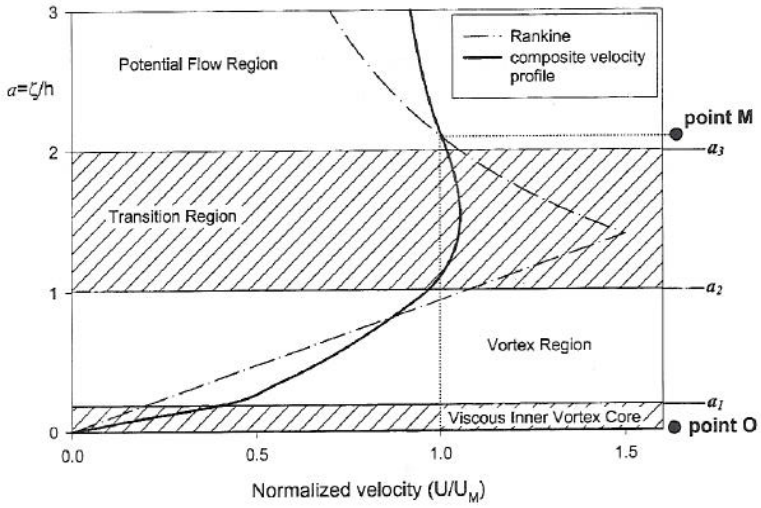

Fig. 6 Velocity profile directly above vortex core through the points O and M

3.1. Radius of curvature

Near the core, $R_c = r$ and $dr = dn$, so Eq. (7) is identical to that for circular flow. As the flow beneath the vortex approaches the roof, however, the radius of curvature must become infinite, since it will be parallel to the flat roof at the surface. Letting $a = (\zeta / h)$ we model $Rc / h = a / (1 + a)$ between the core and the roof $(-1 < a < 0)$. This satisfies these limits, since $R_c \rightarrow -\infty$ as $a \rightarrow -1$ and $R_c / h \rightarrow a$ as $a \rightarrow 0$. The flow will also straighten out above the vortex, eventually merging with the flow curvature associated with the overall flow around the building. A curve-fit to the R_c values calculated for flow above a 2-D surface mounted prism by the CFD code FLUENT yields a relationship of the type $R_c^{upward} / h = a + Ba^C$, where $B = 1$ and $C = 2$. Flow visualization also gives $R_c^{upward} / h = 2a$ at $\zeta = h$.

3.2. Velocity profile

The velocity profile shown in Fig. 6 for $0.2 < a < 1$ is exponential :

$$\frac{U}{U_{a=+1}} = a^{\gamma} \quad \text{where} \quad \gamma = 1/2 . \tag{8}$$

This equation is based upon a curve fit to the velocity profile presented in Rizzi's numerical solution of the complete Navier-Stokes equations for a 65° sweep delta-wing at a 10° angle of attack at $x/c_R = 0.7$ and $M_\infty = 0.85$ (Rizzi and Muller 1989). The fit is shown in Fig. 7a. A similar curve fit is performed with Marwood's rooftop LDV data in Fig. 7b, where U_{max} is not known, so the data is normalized by $U(h/2)$. A power law curve fit was chosen in part because the velocity profile in the core is expected to have a structure similar to that of a turbulent boundary layer, with a viscous inner core, a log-layer, and a defect layer, and such profiles are often represented by a power-law relationship. Note that if $U = C_1\sqrt{a}$ is substituted into Eq. (7), the pressure is seen to vary linearly with a, $P = \rho C_1^2 a$. This linear variation agrees well with data reported in several numerical simulations, adapted for Fig. 8 (The pressure values decrease less rapidly beneath the core because the radius of curvature increases more quickly towards the roof surface, as noted above).

Near enough to the core, viscosity is expected to dominate, so the flow must rotate as a solid body, as in the Rankine vortex, with $U \propto r$.

In the potential flow region, both the Bernoulli equation and Eq. (7) must be obeyed. Using the assumed radius of curvature $R_c(\zeta)$, the velocity profile can be calculated :

$$P = P_\infty - \frac{1}{2}\rho U^2 \qquad \therefore \frac{dP}{dn} = -\frac{1}{2}\rho\frac{dU^2}{dn}$$

Substitute this into Eq. (7) to get

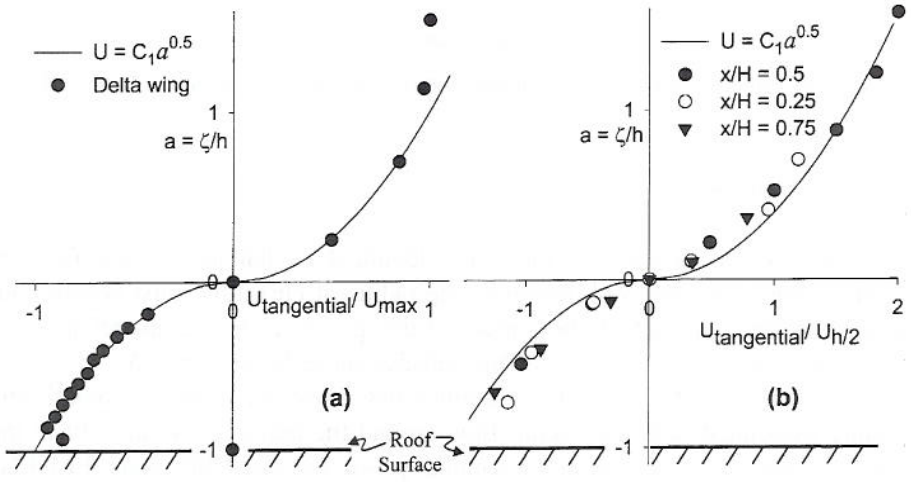

Fig. 7 Mean velocity profiles from surface up through vortex core, with exponential curve fit, for : (a) 65° - sweep delta wing at 10° angle of attack (Rizzi 1989) (b) several planes along a low-rise building model (Marwood 1996)

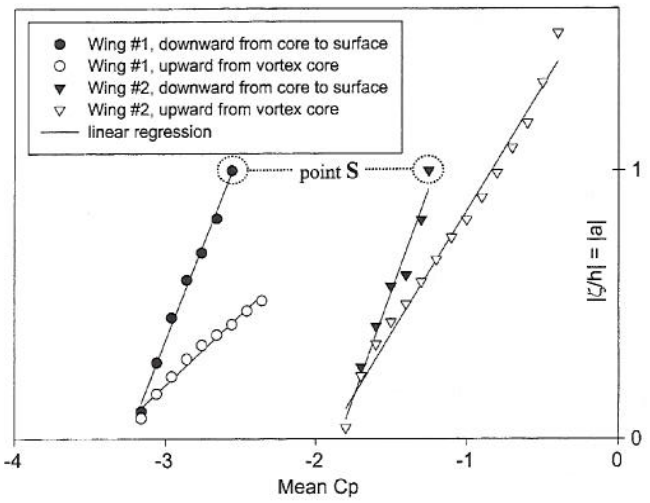

Fig. 8 The nearly linear relationship between pressure drop and distance from the vortex core. Note differing pressure drop rates above and below the core. Data was taken along the line S-M through pressure contours from numerical simulations of delta wing vortices. Wing #1 : Sweep = 75°, angle of attack = 50°, distance along chord = 60% (from Ekaterinaris and Schiff 1994). Wing #2 : Sweep = 76°, angle of attack = 20.5°, distance along chord = 81% (from Kandil and Chuang 1990)

$$-\frac{1}{2}\rho\frac{dU^2}{dn'} = \frac{\rho U^2}{(R_c/h)} \quad \text{where} \quad n' = n/h$$

Isolate the variables and integrate each side to get

$$\int_{a_3}^{a}\frac{1}{U^2}dU^2 = \int_{a_3}^{a}\frac{-2}{(R_c/h)}dn'$$

where a_3 is the normalized radial distance from the core centre to the start of the potential flow region (assumed to be $2h$). Solving the integral gives

$$\ln(U^2) - \ln(U_3^2) = \int_{a_3}^{a}\frac{-2}{(R_c/h)}dn' \quad \text{or} \quad \frac{U}{U_3} = \sqrt{e^{\left(\int_{a_3}^{a}\frac{-2}{(R_c/h)}dn'\right)}}$$

In the transition region, a curve has been chosen with a maximum at $a_{\max} = (a_2 + a_3)/2$, where a_2 borders the vortex region. This curve's slope attempts to match those of the neighbouring regions at a_2 and a_3. The full set of velocity profile equations is given in Table 1.

3.3. The vortex as pressure drop amplifier

The pressure drop to the surface is calculated through the integration of Eq. (7) from the point M towards the vortex centre, along the ζ axis :

Table 1 Equations used to draw the composite velocity profile in Fig. 6, where the parameters were estimated to be $a_1 = 0.2$, $a_2 = 1$, $a_3 = 2$, $a_{\max} = 1.5$ and $U_{\max} = 1.05\,U_M$. $U_{a2} = U_{transition}(a_2)$, $U_{a3} = U_{transition}(a_3)$, and $U_{a1} = U_{vortex}(a_1)$.

R_c/h	Range	Description	Velocity equation
$-\infty$	$a = -1$	Roof surface	$U = 0$
$a/(1+a)$	$-a_2 < a < -a_1$	Between roof and vortex core	$U(a) = -U_{vortex}(a) = -U_{a_2} \cdot \sqrt{a/-a_2}$
a	$\lvert a\rvert < a_1$	Viscous vortex core	$U(a) = U_{core}(a) = U_{a_1} \cdot a/a_1$
$a + a^2/2$	$a_1 < a < a_2$	Vortex, above the core	$U(a) = U_{vortex}(a) = U_{a_2} \cdot \sqrt{a/a_2}$
$a + a^2/2$	$a_2 < a < a_3$	Transition region	$U(a) = U_{transition}(a) = \dfrac{U_{\max} \cdot 2 \cdot (a/a_{\max})}{1 + (a/a_{\max})^2}$
$a + a^2/2$	$a_3 < a$	Potential flow region	$U(a) = U_{potflow}(a) = U_{a_3} \sqrt{e^{\int_{a_3}^{a} \frac{-2}{(Rc/h)}\,dn'}}$

$$\int_M^S dP = \int_M^S \frac{\rho U^2}{(R_c/h)}\,da$$

Normalizing by the reference flow head gives

$$Cp_S - Cp_M = 2\int_M^S \frac{U^2(a)}{U_{ref}^2 \cdot (R_c(a)/h)}\,da$$

Normalizing the cross-vortex velocity profile by U_M instead of U_{ref} gives

$$Cp_S = Cp_M - \frac{U_M^2}{U_{ref}^2}\left[2\int_S^M \frac{U^2(a)}{U_M^2 \cdot (R_c(a)/h)}\,da\right]$$

where the integral is reversed to give a positive value. Cp_M can be calculated from the velocity at M using the Bernouilli equation, $P_M - P_{ref} = 1/2\rho\,(U_{ref}^2 - U_M^2)$ since M is in the potential flow region :

$$Cp_M = \frac{P_M - P_{ref}}{\frac{1}{2}\rho U_{ref}^2} = 1 - \frac{U_M^2}{U_{ref}^2}$$

Substituting into the equation for Cp_S yields

$$Cp_S = 1 - \frac{U_M^2}{U_{ref}^2}\left[1 + 2\int_S^M \left(\frac{U}{U_M}\right)^2 \cdot \left(\frac{R_c}{h}\right)^{-1} da\right] \tag{9}$$

where both U/U_M and R_c/h are functions of a.

Let $\Delta Cp = 1 - Cp$, which could be thought of at the difference in Cp relative to stagnation, where $Cp = 1$. At the point M, this is equivalent to the pressure coefficient change due to the increased flow velocity, since $\Delta Cp_M = (U_M/U_{ref})^2$. Letting

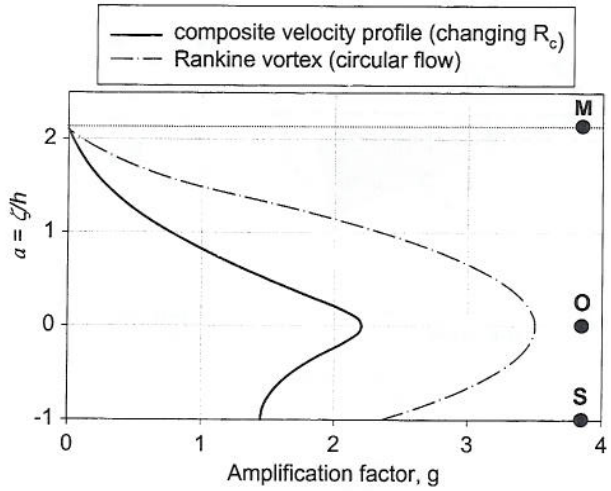

Fig. 9 Vortex amplification factors, showing the effect of reduced curvature

$$g = 2\int_S^M \left(\frac{U}{U_M}\right)^2 \cdot \left(\frac{R_c}{h}\right)^{-1} da$$

gives $\Delta Cp_S = (1 + g) \cdot \Delta Cp_M$. This implies that the vortex can be simply viewed as an amplifier of the velocity related pressure drop at M.

The $g(a)$ profile calculated along the ζ-axis using the $R_c/h(a)$ and $U/U_M(a)$ functions from Table 1 is plotted in Fig. 9, along with the $g(a)$ for circular flow around a Rankine vortex. The figure shows that the total amplification has been reduced (relative to the Rankine pressure drop) by the decrease in curvature (especially in the transition region). An asymmetric "leak" of high amplification from the core to the surface is also evident, since $g(-1) > g(1)$. The leak transfers about half of the vortex core pressure drop (i.e., the drop from $a = 1$ to $a = 0$) to the surface. The pressure loss across the vortex (from $a = 1$ to $a = -1$) can be seen to be roughly equivalent to that across the transition region.

3.4. Effect of wind angle on Cp

The flow model depicted in Fig. 5 is for a 2-d plane normal to the leading edge, so that only a component of the total velocity at M, $U_M \cdot \sin(\alpha)$ is acting to rotate the vortex. The angle α is the wind angle at the point M with respect to the vortex core; it is illustrated in Fig. 10. Experimental measurements taken at CSU using techniques described in the companion paper (Banks and Meroney 2000) show that the wind changes direction as it passes over the leading edge of the roof, shifting to become roughly 10° to 20° more normal to the roof's edge. Since the vortex core is displaced from the leading edge by an angle ϕ_C which is also usually between 10° and 20°, the net effect is that α follows ω fairly closely, as shown in Fig. 11.

Using the full 3-d velocity to calculate the pressure drop at point M, Eq. (9) becomes

$$Cp_S = 1 - \frac{U_M^2}{U_{ref}^2}[1 + \sin^2(\alpha) \cdot g_S] \tag{10}$$

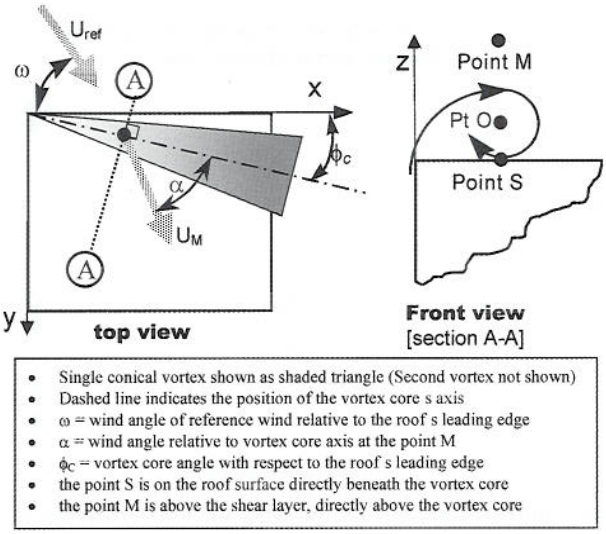

Fig. 10 Nomenclature for model of vortex mechanism. Note that the flow direction changes by an amount $\Delta\omega \approx \phi_C$ as it passed over the roof edge, so that $\omega \approx \alpha$

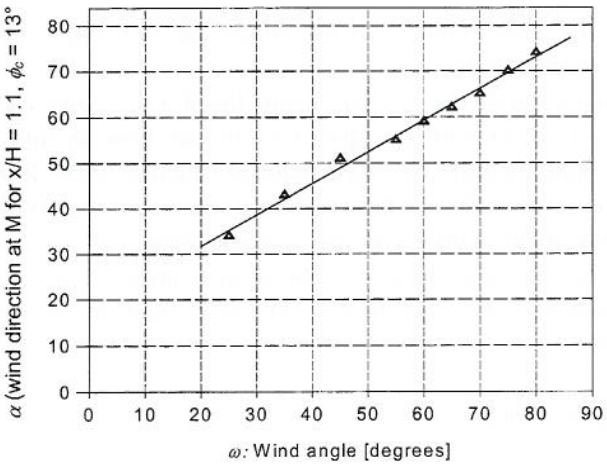

Fig. 11 Wind direction above vortex core, relative to vortex core axis from experiments described by Banks and Meroney (2000)

where g_S is the value of $g(a)$ at the point S and α is a function of ω, as noted above. Eq. (10) can be used to calculate the $Cp\,(a)$ profile along the ζ-axis by using $g(a)$ from Fig. 9. A final comparison with aerospace delta-wing numerical simulation results is shown in Fig. 12, and good agreement is seen between the profile shapes.

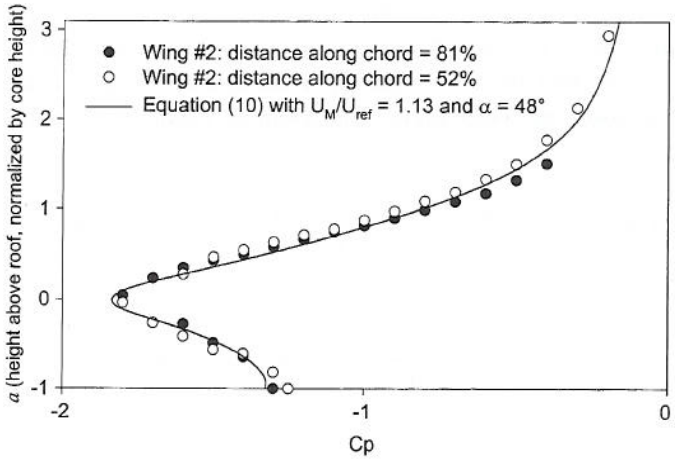

Fig. 12 A comparision of the $Cp(a)$ profiles predicted by Eq. (10) and those for wing #2, a steady-state solution to the Euler equations for a 76° sweep delta wing at an angle of attack of 20.5° (from Kandil and Chuang 1990)

3.5. Incorporating time dependence

3.5.1. A quasi-steady approximation

Visualization of the vortex indicates that for any wind angle, the vortex rapidly and erratically changes its position and size. However, the shape of the vortex is generally self-similar (circular), so provided that the vortex is not "washed out" (absent), it is reasonable to assume that g_S will not depend upon the wind direction. If this is the case, the model's surface pressure predictions can be compared to a measured Cp_S time series by using Eq. (10) to calculate $\overline{Cp}\,(\omega(t))$ for Eq. (1) :

$$Cp_S(t) = \left(\frac{U_{spin}(t)}{\overline{U}_{spin}}\right)^2\left(1 - \frac{\overline{U}_M^2}{\overline{U}_{ref}^2}[1 + \sin^2(\alpha(t)) \cdot g_S]\right) \tag{11}$$

where U_{spin} must be measured at a point near the roof edge, as noted in the introduction. The points M and C have both proven suitable for this purpose.

3.5.2. The intermittency factor

Visualization tests at CSU have shown that as the mean wind angle is increased from $\omega = 20°$ (when the vortex first becomes evident) to $\omega = 90°$ (the case of unstable bubble separation), the vortex becomes increasingly unstable. The instability is evidenced by the vortex erratically disappearing and reappearing. To account for this, an "intermittent vortex factor", $I(t)$, can be introduced to the amplification factor :

$$g(t) = g_S \cdot I(t)$$

where $g_S \approx 1.5$ from Fig. 9 and the mean value of $I(t)$ is expected to be close to 1 for $\omega < 55°$, and to decrease to almost 0 at $\omega = 90°$. It was initially expected that $I(t)$ would function as a delta

function; if the vortex were present, $I_\delta = 1$, otherwise, $I_\delta = 0$. Since the vortex continues to appear sporadically even at $\omega = 90^{o1}$, I_δ could be unity for any wind angle. Data to be presented in the companion paper will show that there is more of a continuum of $g(t)$ values, with a mean and distribution that depends upon the wind angle. The resulting prediction for the surface pressure time series beneath the vortex core is

$$Cp_S(t) = \left(\frac{U_{spin}(t)}{\bar{U}_{spin}}\right)^2\left(1 - \frac{\bar{U}_M^2}{\bar{U}_{ref}^2}[1 + \sin^2(\alpha(t)) \cdot g(t)]\right) \tag{12a}$$

The mean value becomes

$$C\bar{p}_S = \left(1 - \frac{\bar{U}_M^2}{\bar{U}_{ref}^2}[1 + \sin^2(\bar{\alpha}) \cdot g(\bar{\omega})]\right) \tag{12b}$$

4. Discussion

The "speed-up ratio" as flow passes over the downwind separation bubble at the ridge of a steep escarpment is of the order 1.6 (Cook 1985). The speed-up ratio in this case is defined as the ratio of flow speed above the separation bubble (U_C) to that along the same streamline in the undisturbed upstream flow (U_B) (see Fig. 13). If U_B is measured somewhere between 0.3H and 0.5H, and an exponential open country velocity distribution ($\alpha = .14$) is assumed, then U_C / U_{ref} is roughly

$$\frac{U_C}{U_{ref}} = \frac{U_C}{U_B} \cdot \frac{U_B}{U_{ref}} = 1.6 \cdot \left(\frac{z_B}{z_{ref}}\right)^{.1.4} = 1.4$$

Measurements taken for this experiment and described in the companion paper confirm this estimate, giving $U_M / U_{ref} = 1.42$ for $x / H = 0.38$. It is also shown in the companion paper that while $g > 1.5$ for a strongly re-attaching vortex, weaker re-attachment can lower g considerably. This is not too surprising, since g should be 0 if there is no reattachment and no vortex. Using $\bar{g} = 0.9$ and $\bar{\alpha} = 60°$ in Eq. (12a) gives

$$C\bar{p}_S = (1-(1.42)^2[1+\sin^2(60^o) \cdot 0.9)]) = -2.5$$

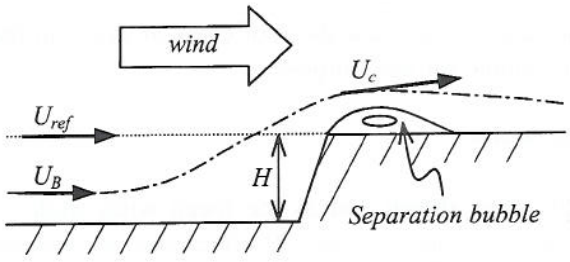

Fig. 13 Flow over a steep escarpment

[1] Experimental results at CSU indicate that the flow in this apparently two dimensional case is actually very three dimensional, with circulating flows, or small, unstable vortices, being shed from the leading edge erratically. These flow structures cause the greatest surface suctions within the bubble, confirming results reported by Saathoff and Melbourne (1989). They generally travel away from the leading edge, but can also move laterally in either direction.

which, as noted in section 2.3, is the mean Cp for tap 50501 at $\omega = 60°$. If we assume that peak suctions of $Cp = -11$ coincide with a strong vortex ($g(t) = 1.7$) and a momentary shift in wind direction to $\alpha(t) = 80°$, the Eq. (12b) gives

$$\left(\frac{U_{spin}(t)}{\overline{U}_{spin}}\right)^2 = \frac{-11}{1-(1.42)^2[1+\sin^2(80^o)\cdot 1.7]} = 1.6.$$

Gusts of this size become increasingly likely as σ_U/U increases, so the likelihood of large negative peak pressures ought to increase as well. This has been observed: peak Cp's below -10 at tap 50501 are seldom seen when $\sigma_U/U < 20\%$, but are relatively common for $\sigma_U/U > 20\%$ (Tieleman *et al.* 1996).

As noted in section 2.3, a 20% turbulence intensity at roof height implies that $U_{ref}(t) > 1.6\overline{U}_{ref}$ for gusts of $U(t) > U + 3\sigma_U$, a condition which occurs over 10 times per 15 minute run (when sampled at 10 Hz). We speculate that Cp's below -11 are not this common because these large gusts must coincide with a shift in wind direction toward flow normal to the wall, and $\alpha(t)$ is greater than 75° less that 7% of the time for $\overline{\omega} = 60°$. They must also coincide with the presence of a strong vortex and solid re-attachment, a condition which is increasingly rare as $\overline{\omega} \to 90°$. As a result, peaks of this size are only seen every few runs, rather than several times per run.

Finally, section 2.3 also indicated that $U_S(t)$ would have to exceed 3.5 times the reference flow velocity to achieve a Cp of -11 if the point vortex model and its direct application of Bernoulli's equation were to apply, a condition which seems intuitively unlikely, and has not been observed experimentally. In contrast, The model embodied in Eq. (12a) requires a maximum velocity of only $2.4U_{ref}$ for such an event: Since $U_{\max} \approx 1.05\ U_M$ (Fig. 6), the ratio can be calculated as

$$\frac{U_{\max}(t)}{\overline{U}_{ref}} \approx \frac{U_{\max}}{U_M} \cdot \frac{U_M}{U_{ref}} \cdot \frac{U_{ref}(t)}{\overline{U}_{ref}} = 1.05 \times 1.42 \times 1.6 = 2.4.$$

5. Conclusions

Existing conical vortex flow and surface pressure models are shown to provide bell-shaped curve fits to the surface pressure profiles. To provide greater insight into the connection between upstream flow and surface pressures beneath the conical vortices, a model of the mechanism by which the roof-top conical vortices create large suctions on the roof surface has been developed.

The model describes how the curving vortex flow causes extremely low pressures at the vortex core. The flattening of the flow beneath the vortex due to the presence of the roof surface causes some of this low pressure to act on the roof surface. The faster the vortex spins, the lower the core pressure and the lower the surface pressure. In this sense, the vortex can be seen as an amplifier of the local pressure drop due to wind gusts.

The model connects surface pressures to the upstream flow in three ways. First, the speed of the vortex spin is determined by the flow velocity component normal to the roof edge, so that the presence of lateral velocity fluctuations will affect the surface pressure through $\alpha(t)$. Second, regardless of wind angle, the pressure above the vortex will be controlled by the speed of gusts passing over the roof corner ($U_{spin}(t)$); the nature of these gusts will clearly be a function of the upstream flow. Finally, the model includes a parameter (g) which describes the quality or strength of the vortex. The value of g could be related to the nature of the re-attachment, which is in turn

affected by the presence of small-scale turbulence (on the order of the width of the shear layer, < H/10).

Experiments designed to validate this model have been performed, and the results are reported in a companion study.

Acknowledgements

The advice of Ivor Banks was greatly appreciated. This work was supported by the US National Science Foundation grant number CMS-9411147 through the CSU-TTU Cooperative Program in Wind Engineering.

References

Banks, D. and Meroney, R. N. (2000), "A model of roof-top surface pressures produced by conical vortices: Evaluation and implications", *Wind and Structures, An Int. J.*, Accepted for publication.

Banks, D., Meroney, R. N., Sarkar, P. P., Zhao, Z. and Wu, F. (2000), "Flow visualization of conical vortices on flat roofs with simultaneous surface pressure measurement", *J. Wind Eng. Ind. Aerodyn.*, **84**(1), 65-85.

Cochran, L.S. and Cermak, J.E. (1992), "Full- and model-scale cladding pressures on the Texas Tech University experimental building", *J. Wind Eng. Ind. Aerodyn.*, **41-44**, 1589-1600.

Cook, N.J. (1985), The designer's guide to wind loading of building structures, part 1., Building Research Establishment, Garston, UK.

Cook, N.J. (1990), The designer's guide to wind loading of building structures, part 2: static structures, Building Research Establishment Report, Garston, UK.

Ekaterinaris, J.A. and Schiff, L.B. (1994), "Numerical simulation of incidence and sweep effects on delta wing vortex breakdown", *J. Aircraft*, **31**(5), 1043-1049.

Greenwell, D.I. and Wood, N.J. (1992), "Determination of vortex location on delta wings from surface pressure measurements", *AIAA J.*, **30**(11), 2736-2739.

Hajj, M.R., Janajreh, I.M., Tieleman, H.W. and Reinhold, T.A. (1997), "On frequency-domain analysis of the relation between incident turbulence and fluctuating pressures", *J. Wind Eng. Ind. Aerodyn.*, **69-71**, 539-545.

Jordan, D.A., Hajj, M.R. and Tieleman, H.W. (1997), "Wavelet analysis of the relation between atmospheric wind and pressure fluctuations on a low-rise building", *J. Wind Eng. Ind. Aerodyn.*, **69-71**, 647-655.

Kandil, O.A. and Chuang, H.A. (1990), "Computation of vortex-dominated flow for a delta wing undergoing pitching oscillation", *AIAA J.*, **28**(9), 1589-1595.

Kawai, H. (1997), "Structure of conical vortices related with suction fluctuation on a flat roof in oblique smooth and turbulent flows", *J. Wind Eng. Ind. Aerodyn.*, **69-71**, 579-588.

Kawai, H. and Nishimura, G. (1996), "Characteristics of fluctuating suction and conical vortices on a flat roof in oblique flow", *J. Wind Eng. Ind. Aerodyn*, **60**, 211-225.

Kind, R.J. (1986), "Worst suctions near edges of flat rooftops on low-rise buildings", *J. Wind Eng. Ind. Aerodyn.*, **25**, 31-47.

Letchford, C.W., Iverson, R.E. and McDonald, J.R. (1993), "The application of the quasi-steady theory to full scale measurements on the Texas Tech Building", *J. Wind Eng. Ind. Aerodyn.*, **48**, 111-132.

Letchford, C.W. and Marwood, R. (1997), "On the influence of v & w component turbulence on roof pressures beneath conical vortices", *J. Wind Eng. Ind. Aerodyn.*, **69-71**, 567-577.

Levitan, M.L. and Mehta, K.C. (1992), "Texas Tech field experiments for wind loads part 1: building and pressure measuring system", *J. Wind Eng. Ind. Aerodyn.*, **41-44**, 1565-1576.

Lin, J.-X., Surry, D. and Tieleman, H.W. (1995), "The distribution of pressure near roof corners of flat roof buildings", *J. Wind Eng. Ind. Aerodyn.*, **56**, 235-265.

Marwood, R. (1996), "An investigation of conical roof edge vortices", Ph.D.thesis, Lincoln College, University of Oxford, Oxford, UK.

Marwood, R. and Wood, C.J. (1997), "Conical vortex movement and its effect on roof pressures", *J. Wind Eng. Ind. Aerodyn.*, **69-71**, 589-595.

Melbourne, W.H. (1993), "Turbulence and the leading edge phenomena", *J. Wind Eng. Ind. Aerodyn.*, **49**, 45-64.
Rizzi, A. and Muller, B. (1989), "Large-scale viscous simulation of laminar vortex flow over a delta wing", *AIAA J.*, **27**(7), 833-840.
Saathoff, P.J. and Melbourne, W.H. (1989), "The generation of peak pressures in separated / reattaching flows", *J. Wind Eng. Ind. Aerodyn.*, **32**, 121-134.
Tieleman, H.W. and Hajj, M.R. (1995), "Pressures on a flat roof- application of Quasi-Steady Theory", 1995 ASCE Engineering mechanics conference, Boulder , Co.
Tieleman, H.W., Hajj, M.R. and Reinhold, T.A. (1998), "Wind tunnel simulation requirements to assess wind loads on low-rise buildings", *J. Wind Eng. Ind. Aerodyn.*, **74-76**, 675-685.
Tieleman, H.W., Surry, D. and Lin, J.-X. (1994), "Characteristics of mean and fluctuating pressure coefficients under corner (delta wing) vortices", *J. Wind Eng. Ind. Aerodyn*, **42**, 263-275.
Tieleman, H.W., Surry, D. and Mehta, K.C. (1996), "Full/model scale comparison of surface pressured on the Texas Tech experimental building", *J. Wind Eng. Ind. Aerodyn.*, **61**, 1-23.
Wilcox, D.C. (1997), Basic Fluid Mechanics, DCW Industries, Inc., La Canada, California.
Zhao, Z., Sarkar, P.P. and Mehta, K.C. (2000), "Wind flow characteristics and their loading effects on low-rise building roofs", (submitted to) *J. Wind and Structures, An Int. J.*

Notation

a	Normalized z-direction distance from the core
C_1	Arbitrary constant
Cp	Pressure coefficient = $(P - P_{ref}) / q_{ref}$)
Cp_{inner}	Cp in viscous region of a Rankine vortex
Cp_{min}	Minimum pressure coefficient along a given x = constant line (same as Cp_S)
Cp_o	Pressure Coefficient at the vortex core
Cp_{outer}	Cp in inviscid region of a Rankine vortex
Cp_M	Cp at the point M (directly above the vortex core)
Cp_S	Cp at the point S (on the roof surface, directly beneath the vortex core)
C_R	Wing chord length (from apex to trailing edge along centerline)
g	Integral of centripetal acceleration from inviscid region, through core, to roof
g_S	Value of g at the point S
h	Height or distance of the vortex core above the roof surface
H	Building height
k	Arbitrary constant
M_∞	Much number
n	Unit normal to streamline
P	Static pressure
P_∞	Static pressure at the stagnation point (when $U = 0$)
q	Flow head = $1/2\rho U^2$
r	Radial distance from the vortex core
R	Radial distance of border between viscous and inviscid flow in Rankine vortex
R_c	Radius of curvature
t	Time
$\vec{u}$	Flow velocity vector
U	Flow speed
U_{ref}	Flow speed measured upstream at roof height
$U_{\max}$	Maximum mean velocity above the vortex core
$U_{(point)}$	U at the location (point) *ex* : U_C , U_M
x	Distance from the apex or leading corner, along the leading edge
y	Distance from the leading edge, along a line normal to the leading edge
Z	Distance above the roof surface

α	Wind angle above the vortex, relative to the vortex core axis
$\Delta P_{\min}$	P-P_∞ directly beneath the vortex, on the roof surface
ϕ	Angle with respect to roof edge; $\phi_c = \phi$ location of vortex core
Γ	Circulation
ρ	Air density
σ_u	Standard deviation of flow speed
ω	Wind angle; 90° is normal to the leading edge
ξ	Distance from the vortex core, in the y direction
$\xi_{1/2}$	Half width of the y-direction pressure profile
ζ	Distance from the vortex core, in the z direction

- Subscripts generally denote the position in space at which a quantity is measured, i.e., Cp_o is the pressure coefficient at the point O, which is the centre of the vortex core.
- Overbars indicate time averaged quantities.

AK